5.3 Solution-Adaptation Applied to Eulerian Transport

Nash'at Ahmad* and Zafer Boybeyi

School of Computational Sciences
George Mason University
Fairfax, Virginia

1 INTRODUCTION

In recent years there has been a growing interest in the use of unstructured adaptive grids for modeling atmospheric transport and diffusion problems (e.g., Ahmad et al. 2005; Bacon et al. 2000). The unstructured grids provide the ability to discretize complex computational domains with relative ease. The capability to resolve the inherently multi-scale nature of atmospheric flows in a computationally efficient manner (*via* static or dynamic grid adaptation) can also be achieved. In this paper the application of solution-adaptive technique (dynamic grid adaptation) to Eulerian transport is presented. Adaptation criteria are discussed and the improvement in computational speed is demonstrated. A decrease in computational resources while maintaining the accuracy of the solution has obvious benefits for responding to emergency-response scenarios.

The unstructured grid technique has been widely used in other scientific disciplines for discretizing computational domains with complex geometries (Löhner 1987; Baum and Löhner 1989; Löhner 2001). This capability is essential for resolving complex terrain features and shoreline boundaries for mesoscale (Bacon et al. 2000; Boybeyi, et al. 2001) and urban-scale atmospheric modeling (Camelli et al. 2004; Hanna et al. 2002). For flows on the urban and the mesoscale, topographic forcing plays a dominant role in the development of the flow and an accurate representation of the underlying terrain is crucial for maintaining the fidelity of the numerical solution. A high degree of mesh refinement becomes critical in resolving locally driven flows, e.g., in simulating the flow field generated by an urban heat island. In addition, computational efficiency can be achieved by providing variable and continuous resolution throughout the computational domain, with a high mesh resolution only in regions of interest (Gopalakrishnan et al. 2002; Sarma et al. 1999). This feature of unstructured grid technique effectively removes the wave reflection problems that are common in grid-nesting techniques.

* *Corresponding author address:* Nash'at Ahmad, School of Computational Sciences, MS 5B2, George Mason University, Fairfax, Virginia 22030.

e-mail: nahmad6@gmu.edu

In simulating Eulerian transport, the importance of fine mesh resolution is well known (Sarma et al. 1999: Behrens et al. 2000; Ghorai et al. 2000). Coarse mesh resolution introduces excessive numerical diffusion into the solution. The degradation in the solution can be further amplified, if the advected tracers are also chemically reactive. Limitations on computational resources can prohibit the use of high mesh resolution throughout the computational domain. Unstructured grid techniques can be used to minimize the computational overhead while attempting to attain the desirable accuracy in the solution.

2 NUMERICAL SCHEME

The 2D scalar transport equation can be written in the conservative form as:

$$\frac{\partial U}{\partial t}+\frac{\partial F}{\partial x}+\frac{\partial G}{\partial y}=0 \qquad (1)$$

where,

$$U=q, \qquad F=qu, \qquad G=qv \qquad (2)$$

q is the Eulerian tracer, u is the velocity component in the x-direction and v is the velocity component in the y-direction.

The scalar transport equation is solved using a higher-order Godunov-type scheme (Godunov 1959; van Leer 1979) on unstructured meshes in two-dimensions. These finite volume discretizations are conservative and have the ability to resolve regions of steep gradients accurately, thus minimizing dispersion or phase errors in the solution. Eq. (1)-(2) can be written in the integral form as:

$$\frac{d}{dt}\int_{\Omega} U\, d\Omega=-\oint_{\Gamma}(F,G).\vec{n}\, d\Gamma \qquad (3)$$

where, **n** is the unit normal pointing out of the control surface Γ of the control volume Ω. Figure 1 shows the cell-centered control volume, Ω with each of its control surfaces and the unit normals pointing outwards from

the control surfaces. Eq. (3) can be approximated directly:

$$V_{cell}\frac{dU_{cell}}{dt}+\sum_{faces}(F,G)\cdot s=0 \qquad (4)$$

where, V_{cell} is the volume of the control volume (area of the triangle in the case of the two-dimensional triangular mesh), U_{cell} is the cell-averaged value of the conserved quantity U at cell center and s is the control surface area (edge lengths of the triangle in case of the two-dimensional mesh).

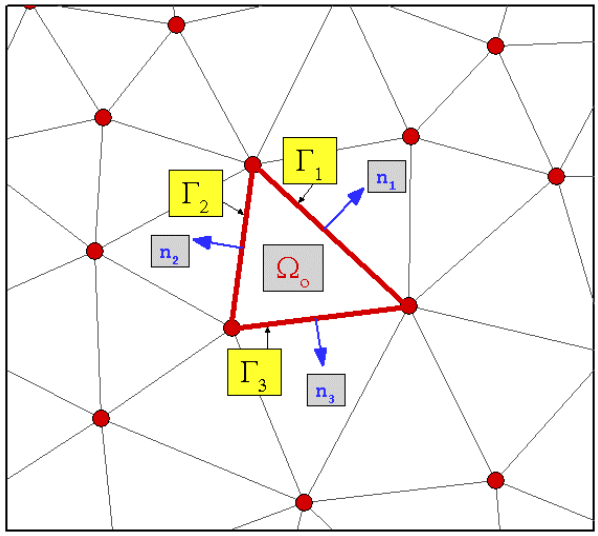

Figure 1: Cell-centered control volume Ω_o and its control surfaces, Γ_i. n_i, are the unit normals.

The advective fluxes are calculated by summing all the incoming and outgoing fluxes through each face of the control volume. The flux across each edge of the cell is calculated using Godunov's method (Godunov 1959). The values on either side of a cell edge form the initial conditions for the Riemann problem. The solution is marched in time within the multi-stage Runge-Kutta explicit time marching scheme (Jameson et al. 1981). In a loop over edges the values of cells on either side of the edge are used to calculate the fluxes. Once the fluxes have been calculated, they are added to the cell centered value in a loop over cells. For the second-order calculation gradient-limited extrapolated values are used in the Riemann solver instead of cell averages (van Leer 1979). Both the Green-Gauss and the Linear Least-Squares gradient reconstruction (Barth and Jesperson 1989) techniques have been implemented to extend the spatial accuracy of scheme to higher-order. The scheme is made TVD (Harten 1983) with the help of slope limiters (Barth and Jesperson 1989; van Leer 1979). The methodology used for dynamically adapting the mesh is described in Ahmad et al. (1998).

3 SOLUTION ADAPTATION

The basic idea behind adaptive mesh refinement is to distribute the error equally over a computational mesh. The regions where numerical error is large are refined to provide better spatial accuracy. The adaptive mesh refinement provides computational efficiency and an attempt can be made to solve computationally intractable problems. Two of the different strategies, which, are commonly used are:

- *H-refinement:* Cells are added in regions where a higher degree of accuracy is required (Löhner 1987).
- *Re-meshing*: The mesh is refined/coarsened and then regenerated. The values from the old mesh are interpolated to the new mesh.

In *h*-refinement the conservation of quantities is easier to maintain during interpolation and computational overhead is also smaller compared to re-meshing (Löhner 2001).

If the exact solution is known then the error-indicator can easily be defined in terms of relative error or a similar quantity. In practice the exact solution is not known *a priori*. The regions of large errors however usually coincide with regions of sharp gradients. There are various ways in which one can define the adaptation criteria (Ahmad et al. 1998; Löhner 1987; Ghorai et al. 2000) depending on the problem. Ahmad et al. (1998) tag cells for refinement based on a Gaussian function around Lagrangian particles. The adaptation criteria (error-indicator) proposed by Löhner (1987) is a function of the Laplacian, first derivatives and differences. Ghorai et al. (2002) have based their error-indicator on the difference between the first and second-order solutions. In the current study three simple error-indicators were used – in the first, the error is based on the gradient. The gradient is normalized by the maximum gradient, which yields a value of error-indicator between 0 and 1. The user specifies a threshold, based on which the cells and their neighbors are tagged for refinement. The user also specifies the maximum and minimum allowable edge lengths. In the second, the maximum difference in adjacent cells is calculated and again the cells are tagged for refinement or coarsening based on a user-specified threshold. Finally an error-indicator is defined based on the difference in derivatives. This method yielded the best results. The second criteria, exhibits some noise which can result in extraneous regions of refinement. In using different adaptation criteria (error indicators), some level of user expertise is needed. Test runs can give the user an idea of what the value of the threshold should be to achieve the desired level of mesh refinement.

Smolarkiewicz flow and the Doswell's problem were simulated to test the implementation of the solution-adaptation techniques.

3.1 Smolarkiewicz Flow

Smolarkiewicz's deformational flow (Smolarkiewicz 1982; Staniforth et al. 1987) is one of the standard tests

for the evaluation of advection schemes (e.g., Sykes and Henn 1995). The flow field is given by:

$$u(x, y) = Ak \sin kx \sin ky \tag{5}$$

$$v(x, y) = Ak \cos kx \cos ky \tag{6}$$

$$k = \frac{4\pi}{L} \tag{7}$$

where, A = 8 and L = 100 units (size of the domain was set to 100x100 units). The radius of the tracer cone was set to 15 units and the height of the cone was 1 unit. The flow field consists of sets of symmetrical vortices. Three simulations were conducted for the Smolarkiewicz flow:

a. **Coarse mesh** consisted of 2488 cells.
b. **Globally refined mesh** consisted of 246498 cells.
c. **Adaptive mesh** consisted of 2488 cells initially. The number of cells increased to 23360 by the end of the simulation. The number of cells is an order-of-magnitude less than the globally refined mesh.

Some of the mesh parameters and the timings for different simulations (final time = 52.752s) are given in Table 1 and the tracer fields for different meshes are shown in Figures 2-4. All simulations were conducted using a higher-order Godunov-type scheme within a 2-stage explicit Runge-Kutta time marching scheme. A CFL criteria of 0.9 was maintained in calculating the time step. For the adaptive run the refinement cycle was invoked every other iteration. The coarsening cycle was turned off.

Table 1: Timings – Smolarkiewicz Flow

case	edgemin	edgemax	time
fine	0.13	0.51	3192.60
coarse	1.59	4.66	1.35
adaptive	0.15	4.66	648.52

Figure 5 shows a comparison with Staniforth's analytical solution for tracer values at y = 50. The Staniforth solution is computed numerically and requires a sampling interval (0.00625 was used in Staniforth et al. 1987). For the comparison shown in Figure 5, a sampling interval of 0.1 was used. The results show that the solution on the coarse mesh becomes too diffusive and the representation of peak concentrations is poor. The adaptive mesh on the other hand reproduces comparable results to the globally refined mesh at reduced computational cost. A further reduction in timing may be achieved by invoking the coarsening cycle and code optimization. It should be noted that the speedup would probably be higher if the number of tracer species is higher.

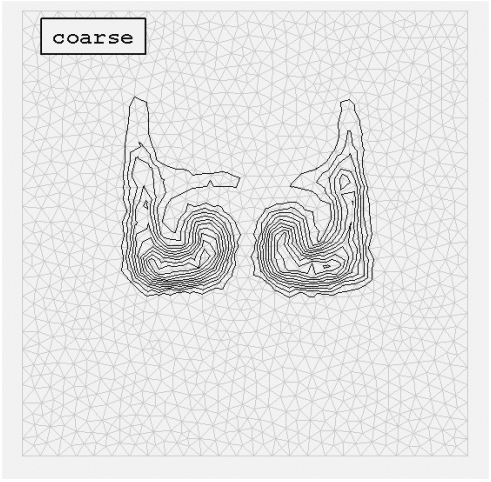

Figure 2: Smolarkiewicz's Deformational Flow. Solution at time = 52.752 s. Coarse mesh.

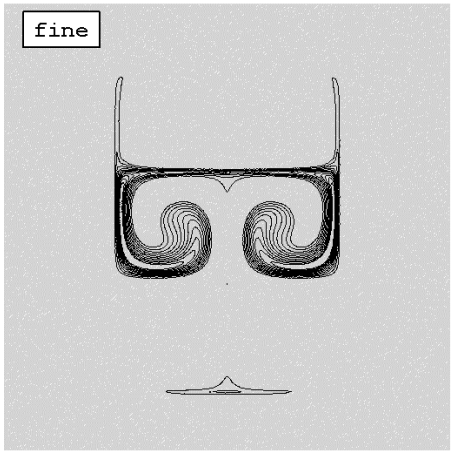

Figure 3: Smolarkiewicz's Deformational Flow. Solution at time = 52.752 s. Fine mesh.

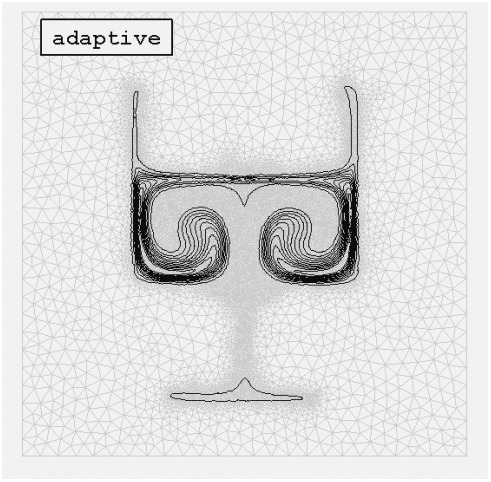

Figure 4: Smolarkiewicz's Deformational Flow. Solution at time = 52.752 s. Adaptive mesh.

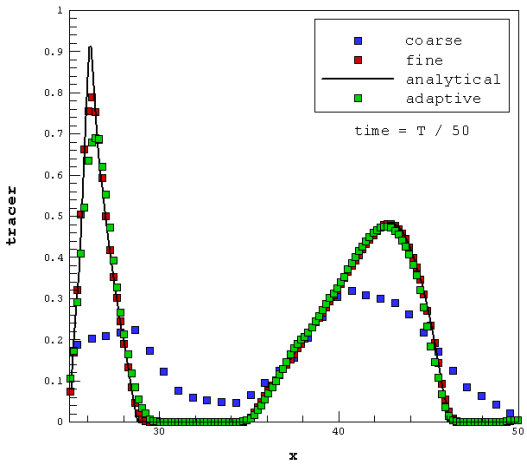

Figure 5: Smolarkiewicz's Deformational Flow. Solution at time = 52.752 s. The values between x = 25 and x = 50 are shown for y = 50. The sampling interval was set to 0.1 for the analytical solution.

3.2 Doswell Test

The simulation of Doswell's cyclogenesis problem (Doswell 1984) is presented in this section. Doswell's idealized model describes the interaction of a nondivergent vortex with an initially straight frontal zone. The flow field for the Doswell test can be defined as follows:

$$u(x,y) = -\frac{y}{r}\frac{f_t}{f_{\max}}; \quad v(x,y) = \frac{x}{r}\frac{f_t}{f_{\max}} \tag{8}$$

where, r is the distance from any given point to the origin of the coordinate system, f_{max} = 0.385 is the maximum tangential velocity and f_t is given by:

$$f_t = \frac{\tanh(r)}{\cosh^2(r)}. \tag{9}$$

The initial tracer field is given by:

$$q(x,y,0) = -\tanh\left(\frac{y}{\delta}\right) \tag{10}$$

where, δ is the characteristic width of the front zone. The value of δ was set to 0.02 for a non-smooth cyclogenesis. The domain was bounded within x:[-4,4] and y:[-4,4], and the simulation was run for t = 4 units. A refinement cycle was invoked every second iteration. Figures 6 shows the initial conditions and Figures 7 and 8 show the results for simulation with no adaptation and with adaptation respectively. By providing a high mesh resolution in the region of high gradients, as the simulation evolved, the sharp interface of the frontal zone was maintained.

Figure 6: Doswell Test. Time = 0 s. Initial conditions.

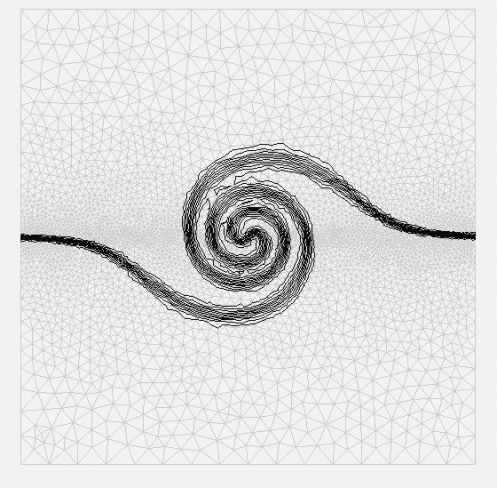

Figure 7: Doswell Test. Time = 4.0s. No adaptation.

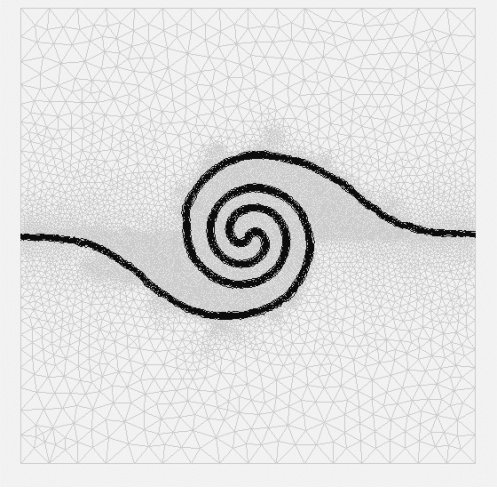

Figure 8: Doswell Test. Time = 4.0 s. Adaptive run.

4 CONCLUSIONS

Solution-adaptive simulations on unstructured grids were presented. It was shown that the technique improves the computational efficiency (5 times speedup for the Smolarkiewicz flow) while maintaining the fidelity of the solution. The scheme also shows promise in resolving and tracking phenomenon characterized by steep gradients at a relatively low computational cost.

Acknowledgement: Many thanks to Drs. Doug Henn and Ian Sykes for providing the analytical solution of the deformational flow test.

REFERENCES

Ahmad, N., Z. Boybeyi, R. Löhner and A. Sarma, 2005: A Godunov-Type Finite Volume Scheme for Flows on the Meso- and Micro-scales. AIAA Paper 2005-1234.

Ahmad, N., D. Bacon, Z. Boybeyi, T. Dunn, M. Hall, P. Lee, D. Mays, A. Sarma and M. Turner, 1998: A Solution-Adaptive Grid Generation Scheme for Atmospheric Flow Simulations. *Numerical Grid Generation in Computational Field Simulations*, Proceedings of the 6th International Conference held at University of Greenwich. 327-335.

Bacon, D. P., N. N. Ahmad, Z. Boybeyi, T. J. Dunn, M. S. Hall, P. C. S. Lee, R. A. Sarma, M. D. Turner, K. Waight, S. Young, and J. Zack, 2000: A Dynamically Adapting Weather and Dispersion Model: The Operational Multiscale Environment Model with Grid Adaptivity (OMEGA). *Mon. Wea. Rev.*, **128**, 2044-2076.

Barth, T. J., and D. C. Jesperson, 1989: The Design and Application of Upwind Schemes on Unstructured Meshes. AIAA Paper 1989-0366.

Baum, J. D., and R. Löhner, 1989: Numerical Simulation of Shock-Elevated Box Interaction Using an Adaptive Finite Element Shock Capturing Scheme. AIAA Paper 1989-0653.

Behrens, J., K. Dethloff, W. Hiller, and A. Rinke, 2000: Evolution of Small-Scale Filaments in an Adaptive Advection Model for Idealized Tracer Transport. *Mon. Wea. Rev.*, **128**, 2976-2982.

Boybeyi, Z. N. Ahmad, D. Bacon, T. Dunn, M. Hall, P. Lee, A. Sarma and T. Wait, 2001: Evaluation of the Operational Multiscale Environment Model with Grid Adaptivity against the European Tracer Experiment. *J. App. Met.* **40**. 1541-1558.

Doswell, C. A, 1984: A Kinematic Analysis of Frontogenesis Associated with a Nondivergent Vortex. *J. Atmos. Sci.*, **41**, 1242-1248.

Camelli, F., R. Löhner, W. C. Sandberg and R. Ramamurti, 2004: VLES Study of Ship Stack Gas Dynamics. AIAA Paper 2004-0072.

Ghorai, S., A. S. Tomlin, and M. Berzins, 2000: Resolution of pollutant concentrations in the boundary layer using a fully 3D adaptive gridding technique. *Atmos. Env.*, **34**, 2851-2863.

Godunov, S. K., 1959: A Finite Difference Method for the Computation of Discontinous Solutions of the Equations of Fluid Dynamics. *Mat. Sb.*, **47**, 357-393.

Gopalakrishnan, S. G., D. Bacon, N. Ahmad, Z. Boybeyi, T. Dunn, M. Hall, P. Lee, R. Madala, A. Sarma, M. Turner, and T. Wait: 2002: An Operational Multiscale Hurricane Forecasting System. *Mon. Wea. Rev.*, **130**, 1830-1847.

Hanna, S., S. Tehranian, B. Carissimo, R. W. Macdonald, and R. Löhner, 2002: Comparisons of model simulations with observations of mean flow and turbulence within simple obstacle arrays. *Atmos. Env.*, **36**, 5067-5079.

Harten, A., 1983: High resolution schemes for hyperbolic conservation laws. *J. Comp. Phys.*, **49**, 357-393.

Jameson, A., W. Schmidt, and E. Turkel, 1981: Numerical Solution of the Euler Equations by Finite Volume Method using Runge-Kutta Time Stepping Schemes. AIAA Paper 1981-1259.

Löhner, R., 1987: An Adaptive Finite Element Scheme for Transient Problems in CFD. *Comp. Meth. Appl. Mech. Eng.*, **61**, 323-338.

Löhner, R., 2001: Applied CFD Techniques: An Introduction based on Finite Element Methods. John Wiley and Sons Ltd.

Sarma, A., N. Ahmad, D. Bacon, Z. Boybeyi, T. Dunn, M. Hall and P. Lee, 1999: Application of Adaptive Grid Refinement to Plume Modeling. Air Pollution VII. WIT Press. 59-68.

Smolarkiewicz, P. K., 1982: The multi-dimensional Crowley advection scheme. *Mon. Wea. Rev.*, **113**, 1050-1065.

Staniforth, A., J. Coté and J. Pudykiewicz, 1987: Comments on "Smolarkiewicz's Deformational Flow". *Mon. Wea. Rev.*, **115**, 894-900.

Sykes, R. I., and D. S. Henn, 1995: Representation of Velocity Gradient Effects in a Gaussian Puff Model. *J. App. Met.*, **34**, 2715-2723.

van Leer, B., 1979: Towards the Ultimate Conservative Difference Scheme. V. A Second-Order Sequel to Godunov's Method. *J. Comp. Phys.*, **32**, 101-136.